

Modeling of shallow landslides in an unsaturated soil slope using a coupled model

Yongmin Kim ^{1a} and Sangseom Jeong ^{*2}

¹ School of Civil and Environmental Engineering, Nanyang Technological University, 50 Nanyang Avenue, Singapore 639798, Singapore

² School of Civil and Environmental Engineering, Yonsei University, 50 Yonsei-ro, Seoul 120-749, Korea

(Received July 07, 2016, Revised January 20, 2017, Accepted March 14, 2017)

Abstract. This paper presents a case study and numerical investigation to study the hydro-mechanical response of a shallow landslide in unsaturated slopes subjected to rainfall infiltration using a coupled model. The coupled model was interpreted in details by expressing the balance equations for soil mixture and the coupled constitutive equations. The coupled model was verified against experimental data from the shearing-infiltration triaxial tests. A real case of shallow landslide occurred on Mt. Umyeonsan, Seoul, Korea was employed to explore the influence of rainfall infiltration on the slope stability during heavy rainfall. Numerical results showed that the coupled model accurately predicted the poromechanical behavior of a rainfall-induced landslide by simultaneously linking seepage and stress-strain problems. It was also found that the coupled model properly described progress failure of a slope in a highly transient condition. Through the comparisons between the coupled and uncoupled models, the coupled model provided more realistic analysis results under rainfall. Consequently, the coupled model was found to be feasible for the stability and seepage analysis of practical engineering problems.

Keywords: shallow landslide; unsaturated slope; coupled hydro-mechanical model; rainfall infiltration; matric suction; Mt. Umyeonsan

1. Introduction

Landslides are common mass-movement processes in mountainous areas and cause geohazard in many parts of the world, particularly on the Korean peninsula, which is covered by residual soils overlying extensively weathered granite (Kim *et al.* 2004, Jeong *et al.* 2008, Kassim *et al.* 2012). Landslides represent a significant threat to human life and infrastructure in most mountainous areas. As an example, South Korea experienced heavy rainfall recorded in June and July 2011. Consequently, 150 small and large landslides occurred in 13 villages near Mt. Umyeonsan. These landslides significantly impacted society because the mountain is located in the central part of Seoul, Korea (Jeong *et al.* 2015). Rainfall-induced landslides are expected to occur more frequently due to an increasing number of extreme weather events (Yasuhara *et al.* 2012, Kim *et al.* 2012, Rahardjo *et al.* 2013).

*Corresponding author, Ph.D., Professor, E-mail: soj9081@yonsei.ac.kr

^a Ph.D., Research Fellow, E-mail: kimkimym@ntu.edu.sg

The rainfall-induced landslides, which frequently mobilizes into destructive debris flows, are commonly shallow with typical depth of slip surface of 1 to 3 m developed parallel along the slope surface (Muller and Martel 2000, Kim *et al.* 2004, Matsushi *et al.* 2006, Chen *et al.* 2012, Huang and Lo 2013). The main reason for slope failures is the loss of matric suction due to rainfall infiltration, and hence cause a reduction in shear strength of unsaturated soils (Fredlund and Rahardjo 1993). The relevant triggering mechanisms of natural slopes comprise of complex hydro-mechanical coupled processes, which depends on the irregular topography, hydro-mechanical properties, and boundary conditions (Iverson 2000, Lu and Likos 2004, Voyiadjis and Song 2006, Sorbino and Nicotera 2013). The degree of saturation and volumetric water content in unsaturated soils may increase under rainfall, inducing the change of permeability function rapidly; at the same time, the alteration of the hydraulic condition, in turn, changes the water flow within the slope and may also alter volumetric response of the soil. During this process, unsaturated soil slopes are vulnerable to lose their overall stability due to the reduction of the shear strength (Laloui *et al.* 2010, Kim *et al.* 2012). It should be pointed out that hydraulic and mechanical properties of unsaturated soils are strongly dependent on each other (Chen *et al.* 2013, Zhang *et al.* 2014). The coupling analysis among the seepage, stress/deformation, and stability is thus vital and has become increasingly important in unsaturated soil mechanics, mainly due to the design requirement and rigorous assessment of slope failures.

Some attempts have been conducted to evaluate the slope stability by coupled hydro-mechanical finite element (FE) analysis. To observe the coupled solid-water-air phenomenon in detail, Khalili and Valliappan (1996), Khalili *et al.* (2004), Gray and Schrefler (2007), Borja *et al.* (2012a), Kim *et al.* (2016) formulated balance equations for a three-phase system consisting of a solid and two immiscible fluids, liquid and gas. Meanwhile, a number of constitutive models for unsaturated soil have been developed based on a combination of experimental observations and theoretical formulations. Alonso *et al.* (1990) developed a constitutive model of Cam-Clay elastoplasticity, which was proposed using the concept of loading-collapse (LC) and suction increase (SI). Their model, known as BBM (Basic Barcelona Model), prompted vigorous study. Many models have been proposed to describe the behavior of unsaturated soils in the various framework (Kohgo *et al.* 1993, Cui and Delage 1996, Loret and Khalili 2002, Borja 2004, Sheng *et al.* 2008, Nuth and Laloui 2008, Zhang and Ikariya 2011, Zhou *et al.* 2012, Song and Yosef 2015). Nevertheless, it can be pointed out that most works have focused on the details of the validation study for their own models. Despite a growing interest in the use of fully-coupled hydro-mechanical models for assessing the behavior of unsaturated slopes (Cho and Lee 2001, Zhang *et al.* 2005, Kim *et al.* 2012, Borja *et al.* 2012b), very few studies have considered actual landslides that resulted in catastrophic damages in the real world (Griffiths and Lu 2005, Borja *et al.* 2012b, Pande and Pietruszczak 2015) because of the uncertainties in the geometry and boundary conditions of the test problem, and difficulties in determining the input parameters for constitutive equations.

This paper presents a case study and numerical investigation to study hydro-mechanical response of a shallow landslide in unsaturated slopes subjected to rainfall infiltration using a coupled model. The coupled model is capable of simultaneously solving stress-strain problems in a deformable solid mixture and water flow in a porous medium. The coupled model was verified against experimental data from shearing-infiltration triaxial tests. For an application purpose, a real case of shallow landslide occurred on Mt. Umyeonsan, Seoul, Korea was simulated and discussed in term of the matric suction, the critical slip surface, and the factor of safety. In addition, the numerical results were compared with those of an uncoupled model and site investigation data to

validate the applicability of the coupled model.

2. Landslide analysis method

A coupled model utilized to analyze the transient problem satisfies balance of mass and balance of linear momentum for solid, water, and air. Owing to the uncertainties in the boundary conditions and material properties, the mathematical formulation assumed the small strain theory, isotropic homogeneous condition, and incompressibility of water, and thus the governing equations are expressed as follows

$$n \dot{S} + S \operatorname{div} v_i = -\operatorname{div} \tilde{v}_i^w \quad (1)$$

$$\operatorname{div} \sigma_{ij} + \rho g_j = 0 \quad (2)$$

where n is the porosity, S is the degree of saturation, v_i is the velocity of the solid, $\tilde{v}_i^w = n^w (v_{i(w)} - v_i)$ is the superficial Darcy velocity, $v_{i(w)}$ is the true seepage velocity, σ_{ij} is the total Cauchy stress, ρ is the total mass density of the solid, g_j is the gravitational acceleration. For the unsaturated zone, the effective stress is calculated from the Bishop stress (1954) but with the effective stress parameter replaced by the effective degree of saturation.

$$\sigma'_{ij} = \sigma_{ij} - \chi p_w \delta_{ij} \quad (3)$$

where $\chi (= S_e)$ is the effective stress parameter, which varies from 0 for dry soils to 1 for saturated soils, p_w is the pore-water pressure, δ_{ij} is the Kroenecker's delta. In this equation, pore-air pressure (p_a) remains equal to the atmospheric value, which is valid at the near-surface condition.

The constitutive equation for unsaturated flow is given by the generalized Darcy's law, relating to the relative velocity of the seepage (\tilde{v}_i^w) with the hydraulic gradient as follows

$$\tilde{v}_i^w = k^w (-\nabla p_w + \rho^{wR} g_j) \quad (4)$$

where k^w is the intrinsic permeability and ρ^{wR} is the intrinsic mass density of water. In this equation, the intrinsic permeability depends on the degree of saturation and porosity as follows

$$k^w = k_{rw}(S) k_{sw}(n) \quad (5)$$

$$k_{rw}(S) = \sqrt{S} \left(1 - (1 - S^{-m})^m \right)^2 \quad (6)$$

$$k_{sw}(n) = \frac{l^2}{\eta_w} \frac{\delta(n)}{\delta(n_0)} \quad (7)$$

where $k_{rw}(S)$ is the relative permeability for unsaturated soils, $k_{sw}(n)$ is the saturated permeability, l^2 is the pore geometry parameter, η_w is the dynamic viscosity of water, $\delta(n)$ is known as the Kozeny-Carman formula (Coussy 2011) for representing the porosity-dependence of permeability, and n_0 is the initial porosity. The constitutive equations for solid deformation relates the effective

Cauchy stress and strain through the tangent stress-strain tensor as follows

$$\sigma'_{ij} = c_{ijkl} \varepsilon_{kl} \quad (8)$$

where c_{ijkl} is the fourth-order tangent stress-strain tensor that depends on the specific constitutive model for the solid, ε_{kl} is the small strain tensor for the solid.

The soil-water characteristics curve (SWCC) relating to the dimensionless volumetric water content (θ) and matric suction (s) provides an important constitutive relationship that is used for the balance of mass and the balance of linear momentum for solid in the unsaturated zone. In this paper, the following equation as defined by van Genuchten (1980) was employed

$$\theta = \theta_s + (\theta_s - \theta_r) \left[1 + (\alpha s)^n \right]^{-m} \quad (9)$$

where the subscript s and r indicate the saturated and residual values, respectively, of the volumetric soil water content θ ; s is the matric suction; and α , n , and m are the curve fitting parameters for SWCC.

The calculation of the factor of safety based on the stress field obtained from the coupled hydro-mechanical simulations can be a significant contribution of this paper in assessing the instability of a slope. In order to determine the minimum factor of safety, the global factor of safety F_s was calculated using the following equations (Cho and Lee 2001)

$$F_s = \frac{\int_{\Gamma} \tau_f d\Gamma}{\int_{\Gamma} \tau_i d\Gamma} \quad (10)$$

$$\tau_f = c' + \sigma'_n \tan \phi' + (p_a - p_w) \tan \phi^b \quad (11)$$

$$\tau_i = 0.5(\sigma_y - \sigma_x) \sin 2\alpha + \tau_{xy} \cos 2\alpha \quad (12)$$

$$\sigma'_n = \sigma_x \sin^2 \alpha + \sigma_y \cos^2 \alpha - \tau_{xy} \sin 2\alpha \quad (13)$$

where τ_f is the shear strength, τ_i is the mobilized shear stress at each gauss point, Γ is the length of the slip surface, σ'_n is the net normal stress on the slip surface ϕ^b is an angle that defines the increase in shear strength for an increase in matric suction, α is the angle of the slip surface to the horizontal plane, and σ_x , σ_y , and τ_{xy} are the calculated stresses on the slope. The minimum local factor of safety determines the critical slip surface that can be predicted as a noncircular curve along the potential failure surface.

3. Verification

Triaxial tests on unsaturated specimens under shearing-infiltration (SI) conditions (Rahardjo *et al.* 2009) were simulated by the coupled model. The soil used in the experiments was kaolin from Kaolin Malaysia SDN BHD. Compacted specimens at a dry density of 1.35 Mg/m³ and a water

content of 21.7% were used in the experiments. The dimensions of the specimen were 100 mm in height and 50 mm in diameter. The static compaction method was used in order to obtain identical specimens with a uniform density along the specimen. SI test consisted of saturation, consolidation, matric suction equalization, shearing, and infiltration stages. The soil specimen was first saturated under zero net normal stress until a pore-water pressure parameter (B) of at least 0.95 was reached. The soil specimen were then consolidated under a specified net confining pressure until no further volume changes were observed. Matric suction equalization stage was conducted under a constant matric suction. After the soil specimens reached equilibrium, the soil specimen was sheared using a strain rate of 0.0008 mm/min until the shear stress of the soil specimens reached 85-90% of the peak deviator stress (Han 1997). The pore-water pressure and the pore-air pressure must be under drained conditions during shearing. In the infiltration stage, water was injected from the base at a constant rate of 0.04 mm³/s. The deviator stress was simultaneously maintained constant and therefore, there was no shear strain applied to the specimen. Nanyang Technological University (NTU) mini suction probes were used to obtain matric suctions in a soil specimen during the tests. Three NTU probes were installed at 3/4 (i.e., top), 1/2 (i.e., middle), and 1/4 (i.e., bottom) heights of the specimen from its base and 120° apart in the radial direction since the matric suction vary with height of the specimen and time. Note that during water injection to the specimen, the pore-air pressure was under a drained condition. The net confining pressure applied on soil specimen was 200 kPa and the matric suctions applied on soil specimen were 50 kPa, 100 kPa and 200 kPa during shearing-infiltration tests.

In the simulation, the full size of the 2D plain strain was considered because the infiltration and loading condition in vertical direction is not affected by symmetric geometry. A coupled finite element (FE) mesh and the applied boundary conditions are shown in Fig. 1. For a consolidation stage, the isotropic stress state was simulated by applying a normal stress on the top and on the right side of the soil specimen equal to initial net confining pressure of 200 kPa. In addition, the desired matric suction state was isotopically simulated by applying a negative pore-water pressure at the pore-water pressure nodes. The consolidation stage was set as the initial condition for the subsequent simulations involving shearing and infiltration. The shearing stage of the coupled analysis was simulated as a stress controlled test. Prior to the infiltration stage, the soil specimen

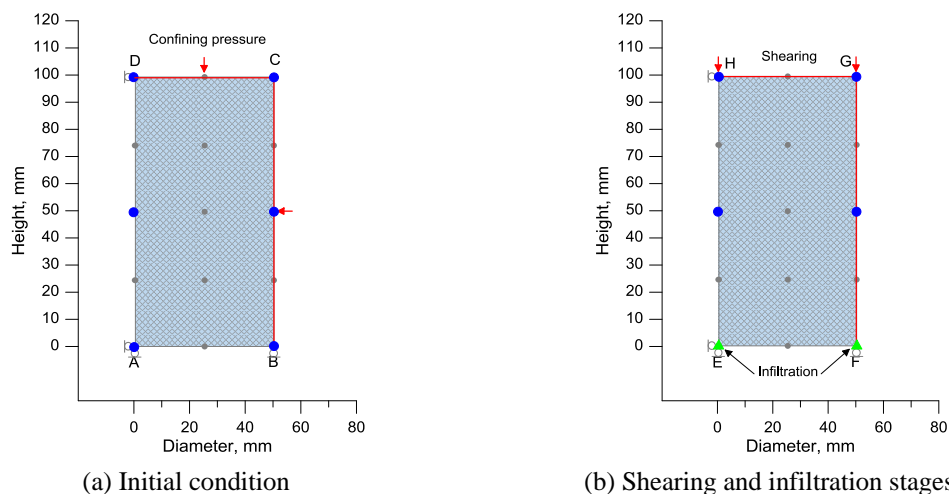


Fig. 1 2D plane strain FE model and numerical analysis procedure for a triaxial shearing-infiltration test

was sheared to 85% of peak shear stress as obtained from the consolidated drained test. The 85% of peak shear stress was chosen as the shear stress in steep slopes under field condition can reach 85% to 90% of peak shear stress (Rahardjo *et al.* 2009). The infiltration stage was simulated by applying positive value of total flux on the bottom of the soil specimen.

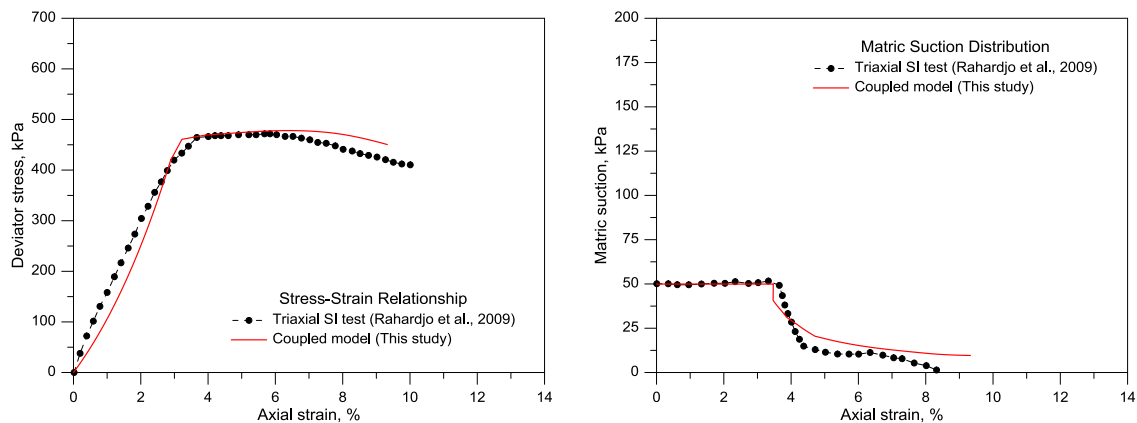
The response of the unsaturated specimen was prescribed by an isotropic, elastoplastic constitutive model using the Modified Cam Clay (MCC) criterion (Borja 2004) with normally

Table 1 Hydraulic properties used for comparison with shearing-infiltration triaxial test

Type	Value
Saturated volumetric water content, θ_s	0.51
Residual volumetric water content, θ_r	0.21
Fitting parameter, α (1/kPa)	0.024
Fitting parameter, n	1.77
Saturated permeability, k_s (m/s)	6.4×10^{-8}
Residual degree of saturation, S_r	0.151

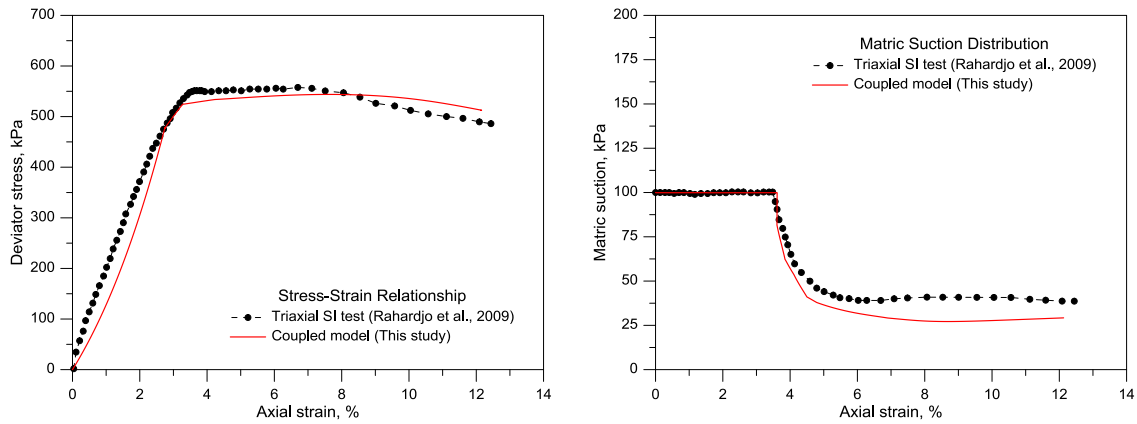
Table 2 Mechanical properties involved in modified Cam Clay model

Type	Value
Virgin compressibility soil index, λ	0.13
Elastic compressibility index, κ	0.018
Slope of critical state line, M	1.05
Dimensionless parameter of suction, k	0.60
Poisson's ratio, ν	0.33
Initial preconsolidation pressure, p_c (kPa)	90
Reference void ratio at p_c , N	1.12

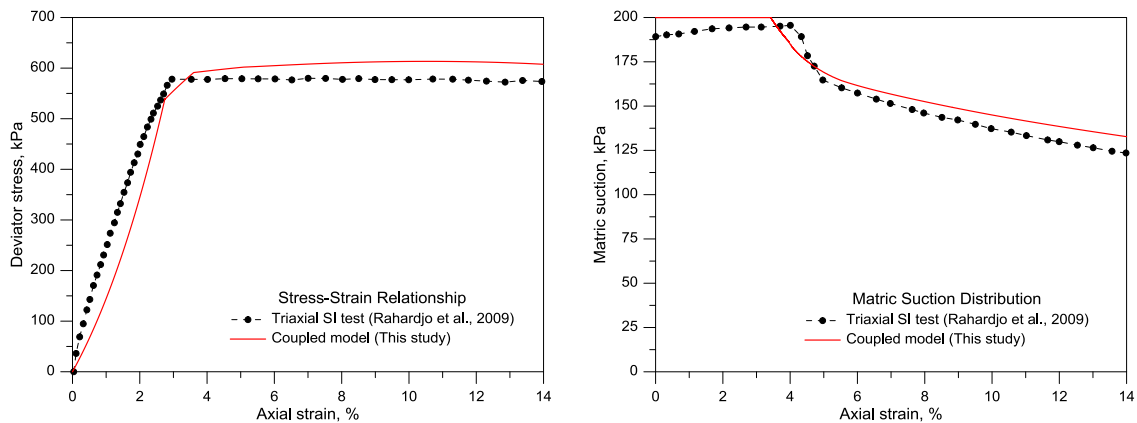


(a) Matric suction = 50 kPa

Fig. 2 Comparison between tests and simulated results of unsaturated specimen under shearing-infiltration condition (tested by Rahardjo *et al.* 2009)



(b) Matric suction = 100 kPa



(c) Matric suction = 200 kPa

Fig. 2 Continued

consolidated condition. The hydraulic properties involved in the coupled model are listed in Table 1. The mechanical properties of the unsaturated soil specimen are listed in Table 2. Meilani (2004) suggested method was adopted for calibration of the material properties.

Fig. 2 shows the comparison between the test and simulated results of the unsaturated soil specimen under shearing-infiltration conditions. The dashed lines are the test results and the solid lines are the simulations. It was confirmed by the comparisons that the simulation can describe the triaxial SI tests in a satisfactory accuracy on the whole. As can be seen in the left figures, the deviator stress could not be maintained, which dropped gradually after failure due to the water infiltration. As can be seen in the right figures, decreases in matric suction in response to changes in axial strain were observed during the water infiltration stage. As expected, in general, the tests and simulated results describe the triggering mechanism of unsaturated soil slopes.

4. Modeling of the Mt. Umyeonsan Landslide in Seoul, Korea

4.1 Study area

The study area of Mt. Umyeonsan is located in the central part of Seoul, Korea. This site is positioned at latitude of 37°28'2"N and longitude of 127°0'25"E with an elevation of approximately 50 to 312.6 m above sea level. Mt. Umyeonsan comprises of steep hills, gullies, and valleys and is topographically characterized by pre-Cambrian metamorphic gneiss associated with the Gyeonggi massif. The majority of the mountain area consists of lacustrine biotite gneiss, which is intensely weathered and decomposed. In this area, small landslides and debris flows frequently occur during the rainy season. Two typhoons, i.e., Typhoon Meari (June 22 to June 27) and Typhoon Muifa (July 28 to August 9), struck the Mt. Umyeonsan area in 2011. When the rainfall from these typhoons exceeded the average rainfall, the most catastrophic recorded landslides and debris flows occurred on Mt. Umyeonsan on July 27, 2011 because Mt. Umyeonsan is completely encircled by buildings, roads, and residential areas.

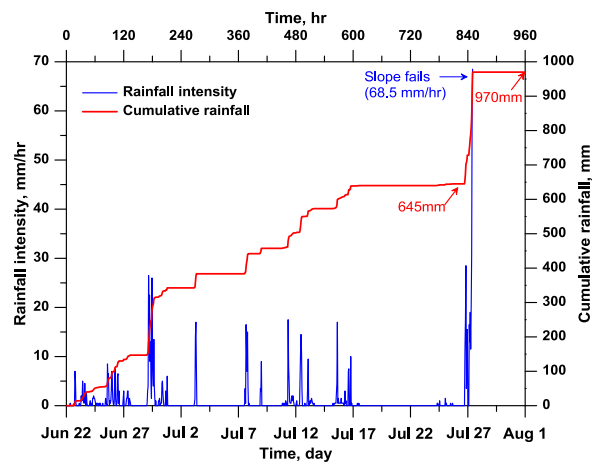


Fig. 3 Hourly and cumulative rainfall from June 22 to August 1, 2011 recorded at Seocho station

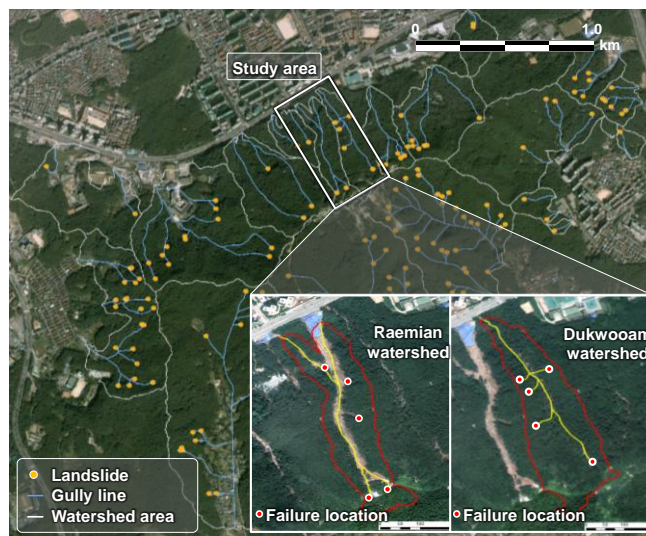


Fig. 4 General view of landslides in 2011 and selected study areas

Fig. 3 shows the hourly and cumulative rainfall for Jun 22 to Aug 1, 2011, recorded by the rain gauges on the Seocho station where is close to the study area. The cumulative rainfall was 970 mm and the maximum hourly rainfall was 68.5 mm, which are not deemed to be particularly high rainfall values. The peak hourly rainfall coincided with the occurrence time of the landslides and debris flows. Fig. 4 illustrates 33 debris flows with 151 landslides in 20 watersheds. The majority of the debris flows streamed downwards to the valley, while the majority of landslides were concentrated on the upper portion of the mountain due to its high slope angle. Among the 20 watersheds, two watersheds (i.e., Raemian and Dukwooram) were selected to investigate the slope instability. Aerial photography was used to examine the locations, number and characteristics of the landslides. Topographic maps and a global positioning system (GPS) were utilized to establish the topography of the debris flows. In addition, geodetic data is used to construct a morphological information, such as the length, channel gradients, and the features at the landslide initiation areas.

4.2 Field and laboratory tests

A comprehensive field monitoring and laboratory tests were initially performed to identify hydraulic and geotechnical information from the near-surface deposits. Fig. 5 shows locations of the boreholes and the test pits in the Raemian watershed. The soil profiles show different strata and depths (6~10 m), and the predominant stratum in the slope consists of colluvium. The sedimentary and weathered soil layers were occasionally interlayered with thin layers. In addition, weathered and soft rock existed in the bottom layer of the slope (see Fig. 6). The geotechnical properties of the colluvial deposits are summarized in Table 3.

To obtain the soil-water characteristic curve (SWCC) of the colluvial deposit, Geotechnical Consulting and Testing Systems (GCTS) pressure plate extractor tests (Pham and Fredlund 2004) and filter paper tests are performed. The results and curve fitting parameters are shown in Fig. 7(a). According to the Unified Soil Classification System (USCS), the colluvial deposit can be classified as CL-SC. The test results showed a high air-entry value and higher saturated and residual volumetric water contents. The SWCC variables was determined using the graphical method. Fig. 7(b) shows the permeability function for the unsaturated soil estimated from the saturated permeability and the measured data using van Genuchten's formulation (1980).

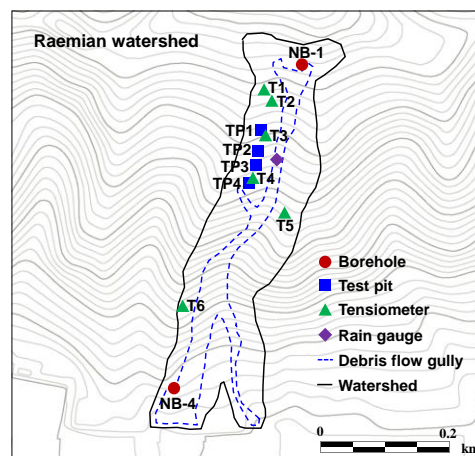


Fig. 5 Location of soil investigation and matric suction monitoring in Raemian watershed

To better understand the hydraulic behavior of the colluvial deposit, the field matric suction was monitored using a jet-fill tensiometer from June 29 to July 27, 2012 at Mt. Umyeonsan. As shown in Fig. 5, a total of 18 tensiometers are installed at different locations (T1-T6) adjacent to the debris flow gullies (only the results for T2 and T5 are presented here). At each location,

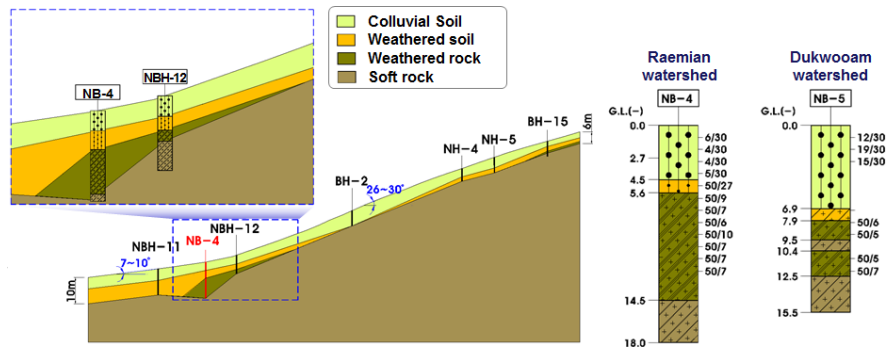


Fig. 6 Cross section of Raemian watershed and soil profiles of selected watersheds

Table 3 Geotechnical properties of colluvial deposit from soil investigations

Type	Test pit 1	Test pit 2	Test pit 3	Test pit 4
Saturated permeability, k_s (m/sec)	4.67×10^{-6}	8.08×10^{-6}	1.99×10^{-6}	3.54×10^{-6}
Water content, w (%)	18.2	14.1	22.1	15.8
Plastic Limit, PL (%)	21.2	22.3	23.7	20.9
Liquid limit, LL (%)	36.6	31.6	40.6	35.9
% Fines (< 0.075 mm)	51.9	28.9	55.7	44.4
Unified Soil Classification System, USCS	CL	SC	CL	SC
Apparent cohesion, c (kPa)	9.2	10.9	11.3	11.8
Internal friction angle, ϕ (deg)	21.7	23.7	23.1	22.7

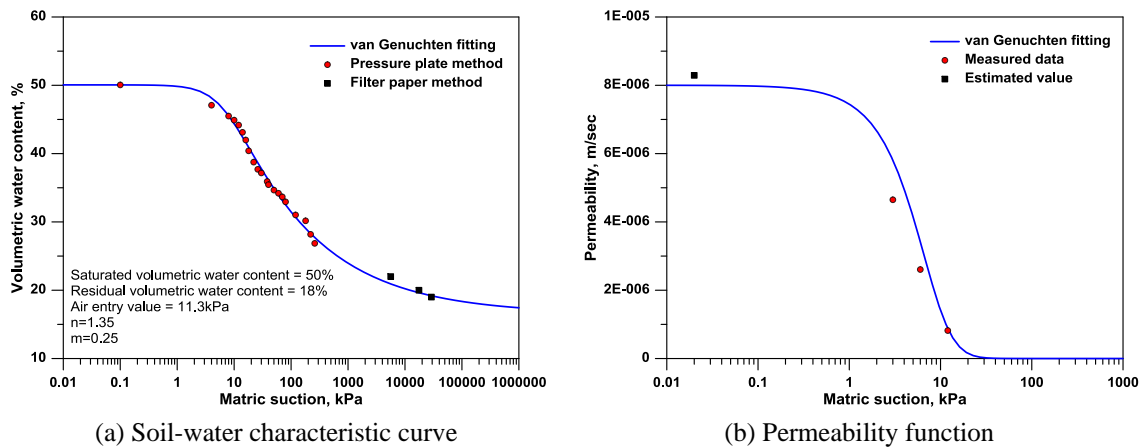


Fig. 7 Unsaturated properties of colluvium from Raemian watershed

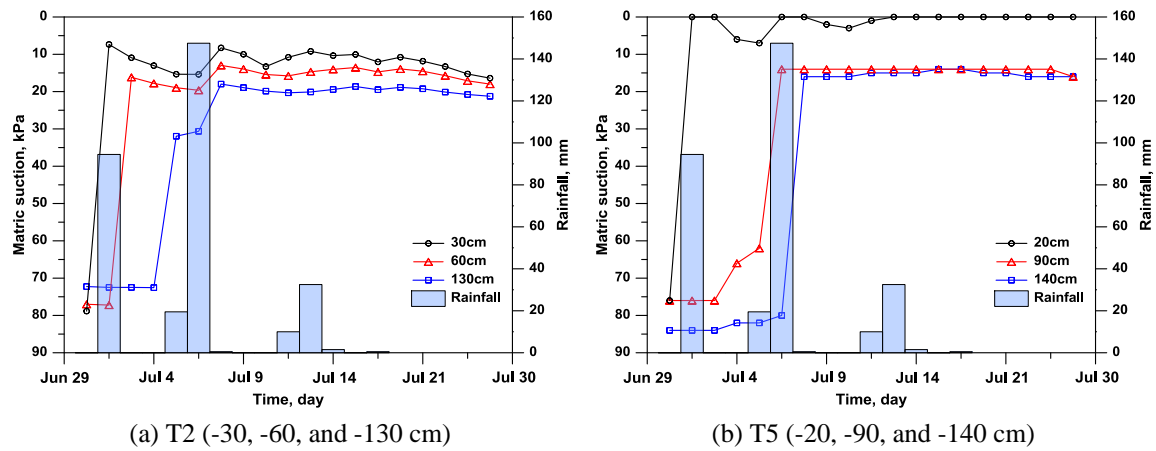


Fig. 8 Monitored matric suction of colluvium adjacent to debris flow gullies in 2012

three tensiometers are embedded within the colluvial layer at depths of 0.3, 0.6, and 1.3 m below the ground surface. Fig. 8 shows the matric suction in response to rainfall events at T2 and T5 locations during the summer period. The initial matric suction is measured at the site on June 29, 2012 prior to the rainy season and varied from 75 to 85 kPa. In addition, the matric suction within the colluvium decreased rapidly after the rainfall began. The matric suction at the 0.3m depth decreases up to zero. At the depth of 0.6 and 1.3 m, the matric suction also decreases, though the effect is delayed and less significant because of the greater depth. Meanwhile, a lower suction value is observed in the upper 0.3 m of the colluvium than in the lower layers, corresponding to higher water contents in the upper layer. This result indicates that the lower suction value results in higher unsaturated permeability, which allows greater downward infiltration of rainwater and indicates the possible formation of preferential local seepage.

4.3 Numerical modeling

4.3.1 Coupled finite element mesh

A two-dimensional (2D) plane strain condition was created on the cross-section of the slope, which passed through the center of the watershed, as shown in Fig. 4. As previously mentioned, the landslides in these areas are initiated in the top of the mountain. The failure locations are confirmed by performing a preliminary study (Jeong *et al.* 2015). Due to uncertainty in the boundary conditions, the geometry problem, and the time-consuming problem, the coupled finite element (FE) mesh was simplified and concentrated on the upper portion of Mt. Umyeonsan. Fig. 9 shows the FE mesh for the Raemian slope and the nine-node quadrilateral mixed finite elements were adopted to incorporate the coupled water flow and soil deformation in the unsaturated soils. In the coupled analysis, the model assumed that the soil consisted of homogeneous colluvium, that the majority of slope failures occurred at shallow depths, and that the underlying bedrock consisted of homogeneous impermeable soft rock.

4.3.2 Model parameters and rainfall data

The initial groundwater table was assumed to be located at the bottom of the bedrock. The initial slope conditions were taken as hydrostatic with initial matric suction of 80 kPa obtained

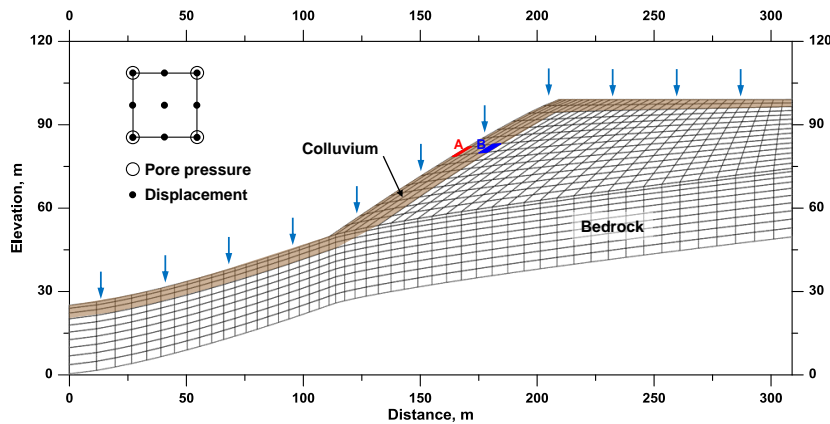


Fig. 9 Finite element mesh used in the coupled model (Raemian watershed)

Table 4 Model parameters used for landslide simulation

Type	Value
Elastic modulus, λ	29×10^6 Pa
Shear modulus, μ	7×10^6 Pa
Shear strength parameters, $\phi^i, \phi^b, \psi^i, c^i$	$22.8^\circ, 15^\circ, 10^\circ, 10.7$ kPa
Plastic parameters, h_c (kPa), β	$10 \times 10^3, -1$ (compression)
Real density of solid, water and air, ρ^{aR} (kg/m^3)	1850, 1000, 1.2
Viscosity of water, η_w (Pa·s)	10^{-3}
Initial porosity, $n = n^w + n^a$	0.41 (= 0.2 + 0.21)
Saturated permeability, k_s (m/sec)	8.0×10^{-6}
Residual degree of saturation, S_r	0.131

from field monitoring. The limit was imposed to prevent the generation of unrealistic pore water pressure. The pore-air pressure was considered atmospheric because of the near-surface condition. Several soil properties related to unsaturated soils, such as the mechanical and hydraulic parameters, are summarized in Table 4. To determine the initial in-situ stress conditions within the slope, a gravity loading stage was used in the coupled model at the beginning of the simulation. Once the initial stresses were computed, the displacements were reset to zero and the coupled hydro-mechanical portion of the simulation begins.

The rainfall data recorded at the Seocho station were used as the flux boundary conditions q (see Fig. 3), which was controlled at the surface of the slope. The total duration of rainfall from June 22 to July 27 was 850 hours (35.4 days) and was divided into several stages to simulate a realistic rainfall event. In addition, a non-ponding boundary condition was adopted to prevent excessive accumulation of rainfall on the slope surface. The nodal flux (Q) of zero was applied along the sides and the bottom of the slope to simulate the no flow zone.

4.4 Results and discussions

4.4.1 Matric suction

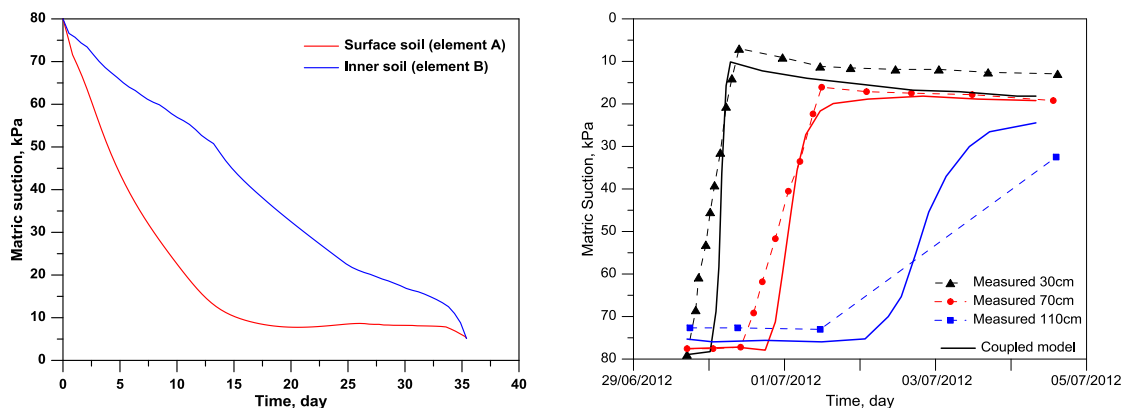
To investigate the mechanism of rainfall-induced slope failure, the variations in the matric

suction was firstly investigated. Fig. 10(a) shows the distribution of matric suction with time for the surficial (element A) and inner (element B) layers within the colluvium as shown previously in Fig. 9. The matric suction in the surficial layer of the colluvium rapidly decreased after the rainfall began, whereas the matric suction in the bottom layer of the colluvium gradually decreased. The discrepancy in the matric suction with time can be attributed to the low permeability of the soil, which results in slow infiltration process. When the infiltration distance is relatively long (element B), more time is required for the rainwater to reach greater depths because the water flow on the slope surface is easily delayed by the soils with lower permeability. The matric suction of both elements eventually converges to approximately 5 kPa as time passed. This result may be attributed to the fact that the colluvial soil contains fine materials (i.e., silty and clay) that range from 28.9 to 55.7%. As a result, decrease in the matric suction in colluvium layer could reduce the shear strength and the capillary tension among the soil particles, and consequently weakens the soil slope.

The field evidence was required to validate the responses of the colluvial soil to rainfall infiltration because the correlation between the variations in matric suction and the mechanism of rainfall-induced slope failure is still exposed to several uncertainties (Kassim *et al.* 2012). The simulated matric suction distribution was compared with those of field measurements (only the result for T1 is presented here) to identify the adequate modeling that best fit the field data set. Fig. 10(b) compares the field matric suction measured at T1 (-30 cm, -70 cm, and -110 cm depths) with dashed lines and the simulated matric suction with solid lines. Average matric suction for four nodes in target element was used in these comparisons. Stiffer responses of the matric suction during rainfall as compared with the field measurements are observed in coupled model. This indicates the limitation of the numerical analysis method used in this study. The complicated distribution of field matric suction, which depends on several surrounding circumstance, cannot be simply simulated through the numerical method in an idealized condition. Although the coupled model has such limitations, the general trend of the measured matric suction is fairly well predicted.

4.4.2 Critical slip surface

For the infiltration characteristics of the soil slope, a critical slip surface was evaluated to



(a) Variation of matric suction at element A and B

(b) Comparison with field matric suction

Fig. 10 Predicted matric suction

investigate slope instabilities and failure zones. Fig. 11 shows noncircular critical slip surfaces in the Raemian and Dukwoom slopes obtained from the coupled model. The critical slip surface gradually deepens towards a bedrock during rainfall. This result indicates that coupled model can simulate the progressive failure of the slope within the colluvium layer as rainwater infiltrates from the slope surface into deeper soil layers. The critical slip surface is consistently developed on the colluvium-bedrock interface at the end of the rainfall. In addition, the geotechnical soil investigations indicated that the colluvial soils are characterized as silty sand. The standard penetration number of the colluvium ranges from approximately 4/30 - 5/30 in Raemian watershed (see Fig. 6). The N-values of less than 10 signify a very soft and loose soil (Bowel 1997). Therefore, it is inferred that the colluvial deposits provide the source material for the landslide and debris flows.

A limit equilibrium solution (GeoSlope International Ltd. 2012) for searching for the critical failure surface was extensively employed in the analysis of slope stability. For comparison purpose,

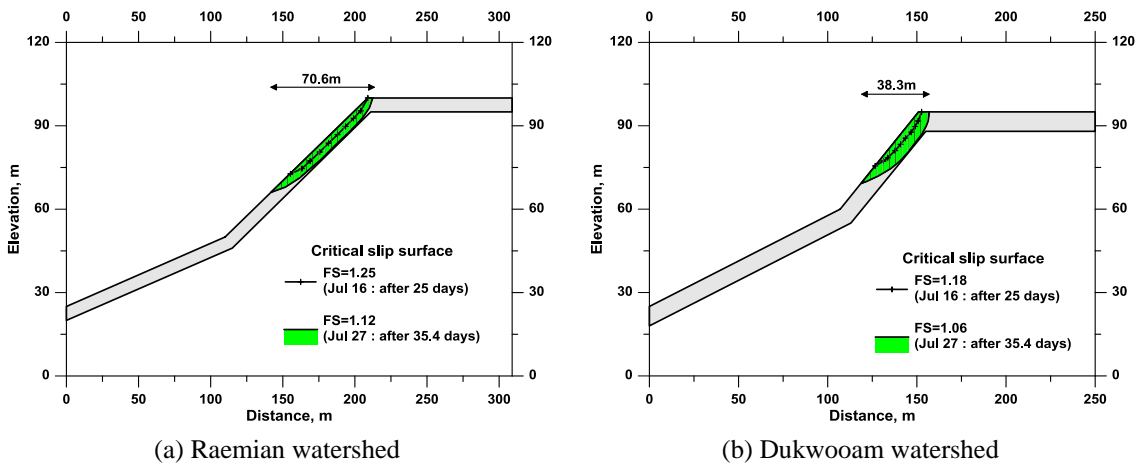


Fig. 11 Critical slip surface of study areas from coupled model

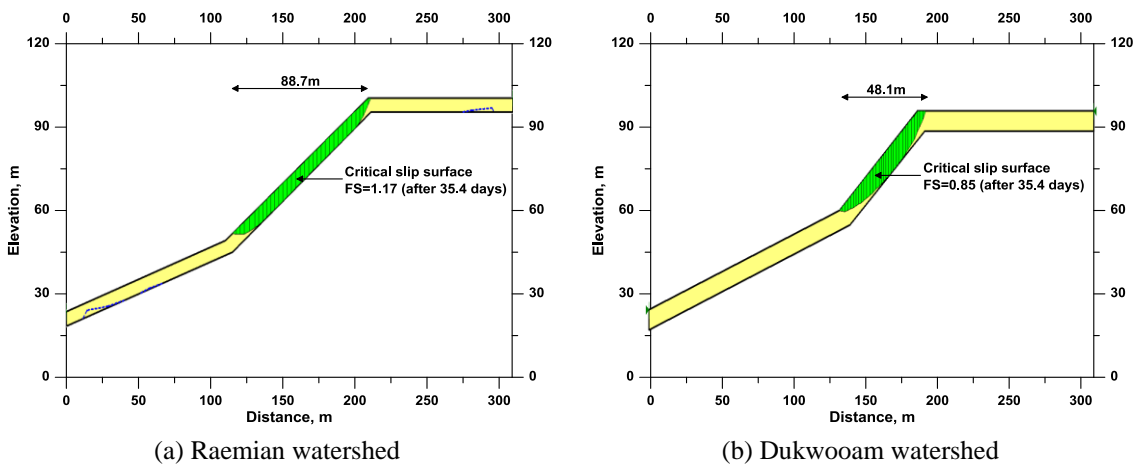


Fig. 12 Critical slip surface of study areas from GeoSlope (SEEP/W and SLOPE/W)

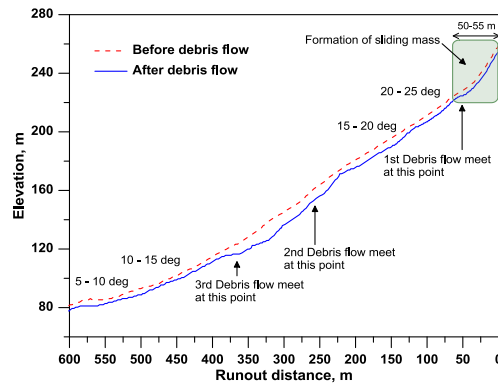


Fig. 13 Longitudinal profile of debris flow gully from LiDAR survey in Raemian watershed

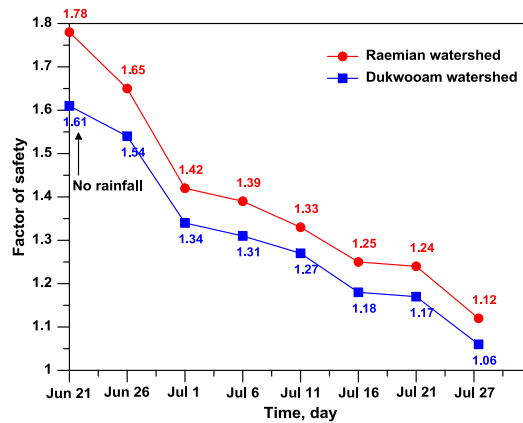


Fig. 14 Variations in factor of safety for Raemian and Dukwooam watersheds

uncoupled analyses (i.e., seepage and slope stability analyses) were performed using SEEP/W and SLOPE/W. Fig. 12 shows the failure surface of the slope, which has the same material properties and boundary conditions with the coupled model. The limit equilibrium analysis could predict the considerably different failure shape and overestimate the failure zone as compared with the coupled model. This could be due to the fact that the limit equilibrium solution provides only one average factor of safety for the critical failure surface without considering the stress-strain distribution in the slope due to rainfall infiltration, whereas the coupled model performed in this study considers the deformation characteristics and inflection points as a failure initiation.

Korean Geotechnical Society (2011) performed the field investigation immediately after the landslides and reported that the scrap zone in Raemian watershed was approximately 50 m long and 30 m wide. In addition, an erosional response of the Raemian slope in Fig. 13 indicated that a weakened zone was formed in the colluvium, causing a noncircular-shaped sliding mass, mainly in the upper portion of slopes. Debris flows were initiated at the toe of sliding mass where multiple debris flows meet at the point of 50-55 m away from the top of the slope. The landslide length of 35 m and width of 20 m in Dukwooam watershed was also investigated using the same technique as applied in Raemian slope. Based on these results, the numerical results from both software show good agreement with the actual scrap zone.

4.4.3 Factor of safety

Fig. 14 shows the variations of the factor of safety in the Raemian and Dukwoam slopes. The factor of safety for both slopes decreased with time, reaching their minimum values at the end of the rainfall events. The initial factor of safety for the Raemian slope is 1.78 during the driest period, which is larger than that of the Dukwoam slope (1.61) due to the different slope angles and soil depths. The factor of safety decreased significantly at the beginning of the rainfall events due to the effect of a reduction in matric suction. When rainwater infiltrated the soil layer, the matric suction decreased rapidly and factor of safety coincidentally decreased. The magnitude and the rate of decrease in factor of safety is also related to the rainfall intensity.

5. Conclusions

In this paper, a coupled model was developed to solve the coupled problem between soil deformation and water flow process on an unsaturated soil slope. The coupled model was verified against experimental data from shearing-infiltration triaxial tests. In addition, a case study and numerical investigation were presented as the application example. The key features of the coupled model and observations are as follows:

- The coupled model for a deformable unsaturated soil properly describes the poromechanical behavior of a rainfall-induced landslide by simultaneously linking seepage and stress-deformation problems.
- From the comparisons between the shearing-infiltration triaxial tests and the simulation, it is found that the coupled model accurately predicts the hydro-mechanical coupled behaviors of the unsaturated soil (e.g., compacted kaolin), specifically, the stress-strain relation and the variations in matric suction at different constant matric suction.
- In the case study, the behavior of the unsaturated soil slope subjected to rainfall infiltration, such as the change of matric suction, the critical slip surface, and the factor of safety, can be simulated on the whole in a monolithically coupled solution in comparison of the simulated results with the measured ones. It is also found that the simulation can well describe progressive failures in a highly transient problem resulting from decreases in matric suction and deepens in critical slip surface during rainfall.
- It is interesting to note that there are differences between the coupled and uncoupled model. Although the uncoupled model is easy to be implemented in the simulation, it tends to overestimate the failure zone, which may lead to wrong conclusion for the stability of unsaturated soil slope and countermeasures. Therefore, the coupled model can be used for detailed and realistic assessment of shallow landslides or slope failures.

Acknowledgments

The research described in this paper was supported by the Natural Research Foundation of Korea (NRF) grant funded by the Korea government (MSIP) (No. 2011-0030040).

References

- Alonso, E.E., Gens, A. and Josa, A. (1990), "A constitutive model for partially saturated soils", *Géotechnique*, **40**(3), 405-430.

- Bishop, A.W. (1954), "The use of pore-pressure coefficients in practice", *Géotechnique*, **4**(4), 148-152.
- Borja, R.I. (2004), "Cam-clay plasticity. Part V: A mathematical framework for three-phase deformation and strain localization analyses of partially saturated porous media", *Comput. Method. Appl. Mech. Eng.*, **193**(48-51), 5301-5338.
- Borja, R.I., Liu, X. and White, J.A. (2012a), "Multiphysics hillslope processes triggering landslides", *Acta Geotechnica*, **7**(4), 261-269.
- Borja, R.I., White, J.A., Liu, X. and Wu, W. (2012b), "Factor of safety in a partially saturated slope inferred from hydro-mechanical continuum modeling", *Int. J. Numer. Anal. Method. Geomech.*, **36**(2), 236-248.
- Bowel, J.E. (1997), *Foundation Analysis and Design*, (5th Edition), McGraw-Hill, Singapore.
- Chen, R.H., Kuo, K.J. and Chien, W.N. (2012), "Failure mechanism of granular soil slopes under high intensity rainfalls", *J. GeoEng.*, **7**(1), 21-31.
- Chen, H., Zhao, Z. and Sun, J. (2013), "Coupled hydro-mechanical model for fractured rock masses using the discontinuous deformation analysis", *Tunn. Undergr. Space Technol.*, **38**, 506-516.
- Cho, S.E. and Lee, S.R. (2001), "Instability of unsaturated soil slopes due to infiltration", *Comput. Geotech.*, **28**(3), 185-208.
- Coussy, O. (2011), *Mechanics and Physics of Porous Solids*, John Wiley & Sons, Inc., New York, NY, USA.
- Cui, Y.J. and Delage, P. (1996), "Yielding and plastic behaviour of an unsaturated compacted silt", *Géotechnique*, **46**(2), 291-311.
- Fredlund, D.G. and Rahardjo, H. (1993), *Soil Mechanics for Unsaturated Soils*, John Wiley & Sons, Inc., New York, NY, USA.
- GeoSlope International Ltd. (2012), *Seep/W User's Guide for Finite Element Seepage Analysis*, GEOSLOPE Int. Ltd., Calgary, Alta, Canada.
- Gray, G.W. and Schrefler, B.A. (2007), "Analysis of the solid phase stress tensor in multiphase porous media", *Int. J. Numer. Anal. Method. Geomech.*, **31**(4), 541-581.
- Griffiths, D. and Lu, N. (2005), "Unsaturated slope stability analysis with steady infiltration or evaporation using elasto-plastic finite elements", *Int. J. Numer. Anal. Method. Geomech.*, **29**(3), 249-267.
- Han, K.K. (1997), "Effect of hysteresis, infiltration and tensile stress on the shear strength of an unsaturated soil", Ph.D. Thesis; Nanyang Technological University, Singapore.
- Huang, C.C. and Lo, C.L. (2013), "Simulation of subsurface flows associated with rainfall-induced shallow slope failures", *J. GeoEng.*, **8**(3), 101-111.
- Hughes, T.J.R. (1987), *The Finite Element Method*, Englewood Cliffs, NJ, USA.
- Iverson, R.M. (2000), "Landslide triggering by rain infiltration", *Water Resour. Res.*, **36**(7), 1897-1910.
- Jeong, S., Kim, J. and Lee, K. (2008), "Effect of clay content on well-graded sands due to infiltration", *Eng. Geol.*, **102**(1), 74-81.
- Jeong, S., Kim, Y., Lee, J.K. and Kim, J. (2015), "The 27 July 2011 debris flows at Umyeonsan, Seoul, Korea", *Landslides*, **12**(4), 799-813.
- Kassim, A., Gofar, N., Lee, L.M. and Rahardjo, H. (2012), "Modeling of suction distributions in an unsaturated heterogeneous residual soil slope", *Eng. Geol.*, **131-132**, 70-82.
- Khalili, N. and Valliappan, S. (1996), "Unified theory of flow and deformation in double porous media", *Eur. J. Mech - A/Solids*, **15**(2), 321-336.
- Khalili, N., Geiser, F. and Blight, G. (2004), "Effective stress in unsaturated soils: review with new evidence", *Int. J. Geomech.*, **4**(2), 115-126.
- Kim, J., Jeong, S., Park, S. and Sharma, J. (2004), "Influence of rainfall-induced wetting on the stability of slopes in weathered soils", *Eng. Geol.*, **75**(3), 251-262.
- Kim, J., Jeong, S. and Regueiro, R.A. (2012), "Instability of partially saturated soil slopes due to alteration of rainfall pattern", *Eng. Geol.*, **147**, 28-36.
- Kim, Y., Jeong, S. and Kim, J. (2016), "Coupled infiltration model of unsaturated porous media for steady rainfall", *Soils Found.*, **56**(6), 1071-1081.
- Kohgo, Y., Nakano, M. and Miyazaki, T. (1993), "Verification of the generalized elastoplastic model for unsaturated soil", *Soils Found.*, **33**(4), 64-73.

- Korean Geotechnical Society (2011), Research contact report: addition and complement causes survey of Mt. Umyeonsan landslide; Korean Geotechnical Society, Seoul, Korea. [In Korean]
- Laloui, L., Ferrari, A. and Eichenberger, J. (2010), "Effect of climate change on landslide behavior", *Geo-Strata September/October*, 36-41.
- Loret, B. and Khalili, N. (2002), "An effective stress elastic-plastic model for unsaturated porous media", *Mech. Mater.*, **34**(2), 97-116.
- Lu, N. and Likos, W.J. (2004), *Unsaturated Soil Mechanics*, John Wiley & Sons, Inc., New York, NY, USA.
- Lu, N., Godt, J.W. and Wu, D.T. (2010), "A closed-form equation for effective stress in unsaturated soil", *Water Resour. Res.*, **46**(5), W05515.
- Matsushi, Y., Hattanji, T. and Matsukura, Y. (2006), "Mechanisms of shallow landslides on soil-mantled hillslopes with permeable and impermeable bedrocks in the Boso Peninsula, Japan", *Geomorphology*, **76**(1), 92-108.
- Meilani, I. (2004), "Shear strength characteristics of a compacted kaolin under infiltration conditions", Ph. D. Thesis; Nanyang Technological University, Singapore.
- Muller, J.R. and Martel, S.J. (2000), "Numerical models of translational landslide rupture surface growth", *Pure Appl. Geophys.*, **157**(6-8), 1009-1038.
- Nuth, M. and Laloui, L. (2008), "Effective stress concept in unsaturated soils: clarification and validation of a unified framework", *Int. J. Numer. Anal. Methods Geomech.*, **32**(7), 771-801.
- Pande, G.N. and Pietruszczak, S. (2015), "On unsaturated soil mechanics – Personal views on current research", *Studia Geotechnica et Mechanica*, **37**(3), 73-84.
- Pham, H.Q. and Fredlund, D.G. (2004), "New apparatus for the measurement of the soil-water characteristic curves", *Proceeding of the 57th Canadian Geotechnical Conference*, Quebec, QC, Canada.
- Rahardjo, H., Meilani, I. and Leong, E.C. (2009), "Shear strength characteristics of a compacted soil under infiltration conditions", *Geomech. Eng., Int. J.*, **1**(1), 35-52.
- Rahardjo, H., Satyanaga, A. and Leong, E.C. (2013), "Effects of flux boundary conditions on pore-water pressure distribution in slope", *Eng. Geol.*, **165**, 133-142.
- Sheng, D., Gens, A., Fredlund, D.G. and Sloan, S.W. (2008), "Unsaturated soils: From constitutive modelling to numerical algorithms", *Comput. Geotech.*, **35**(6), 810-824.
- Song, C.R. and Yosef, T. (2015), "Seepage-heat coupled analysis for estimating phreatic line of an earth dam from temperature profile", *SAGEEP*, Extended paper, Austin, TX, USA.
- Sorbino, G. and Nicotera, M.V. (2013), "Unsaturated soil mechanics in rainfall-induced flow landslides", *Eng. Geol.*, **165**, 105-132.
- Terzaghi, K. (1925), "Principles of soil mechanics, IV—Settlement and consolidation of clay", *Eng. News-Record*, **95**(3), 874-878.
- van Genuchten, M.T. (1980), "A closed-form equation for predicting the hydraulic conductivity of unsaturated soils", *Soil Sci. Soc. Am. J.*, **44**(5), 892-898.
- Voyiadjis, G.Z. and Song, C.R. (2006), *Coupled Theory of Mixtures in Geomechanics with Application*, Springer, 438 p.
- Yasuhara, K., Komine, H., Murakami, S., Chen, G., Mitani, Y. and Duc, D.M. (2012), "Effects of climate change on geo-disasters in coastal zones and their adaptation", *Geotext. Geomembr.*, **30**, 24-34.
- Zhang, F. and Ikariya, T. (2011), "A new model for unsaturated soil using skeleton and degree of saturation as state variables", *Soil Found.*, **51**(1), 67-81.
- Zhang, L.L., Zhang, L. and Tang, W.H. (2005), "Rainfall-induced slope failure considering variability of soil properties", *Géotechnique*, **55**(2), 183-188.
- Zhang, F., Xiong, Y., Zhang, S. and Ye, B. (2014), "Thermo-hydro-mechanical-air coupling finite element method and its application to multi-phase problems", *J. Rock Mech. Geotech. Eng.*, **6**(2), 77-98.
- Zhou, A.N., Sheng, D.C., Sloan, S.W. and Gens, A. (2012), "Interpretation of unsaturated soil behaviour in the stress-saturation space, II: Constitutive relationships and validations", *Comput. Geotech.*, **43**, 111-123.